IEEE Access
Multidisciplinary | Rapid Review | Open Access Journal

Received June 15, 2019, accepted June 21, 2019, date of publication June 26, 2019, date of current version July 11, 2019.

Digital Object Identifier 10.1109/ACCESS.2019.2925131

Design of a High-Speed Solid-Rotor Induction Machine With an Asymmetric Winding and Suppression of the Current Unbalance by Special Coil Arrangements

CHONG DI, ILYA PETROV, AND JUHA J. PYRHÖNEN, (Senior Member, IEEE)
Department of Electrical Engineering, Lappeenranta University of Technology, 53851 Lappeenranta, Finland

Corresponding author: Chong Di (chong.di@lut.fi)

This work was supported in part by the Scholarship from the China Scholarship Council (CSC) under Grant CSC 201706690032.

ABSTRACT High-speed solid-rotor induction machines (IMs) suffer from higher rotor eddy-current losses (as a result of the air-gap flux density harmonics) more than any other type of high-speed machines because of the solid-rotor steel. A double-layer short-pitch asymmetric winding arrangement with prefabricated coils is proposed in this paper to mitigate the solid-rotor losses and enable easier assembly. However, the asymmetric winding also brings some current unbalance because of three-phase asymmetric stator inductances, especially the winding leakage inductances. Current unbalance can cause harmful effects for both the machine and supply, e.g., torque ripples, unbalanced magnetic pulls, and unbalanced thermal loads of the supply network and supply power electronics. Additionally, a three-phase unbalanced current can cause an extra source of electromagnetic emission to the environment, which can be harmful to surrounding electronics and can cause extra eddy-current losses in surrounding solid surfaces (e.g., a metal terminal box). To mitigate the current unbalance, two methods are compared in this paper. The first method is a slight increase of the stator slot height and placing of the coil sides at the top or bottom within the slot height for different phases. The stator slot height is optimized based on the 2-D finite-element method (FEM) to achieve the best solution for mitigation of the current unbalance. The other method is based on the results of the first method, and the coil side position for a specific phase is further adjusted. Unlike conventional methods of mitigating the current unbalance by power electronics, the proposed method suppresses the current unbalance solely by adjusting the machine design, which avoids extra investments for power electronics devices. In addition, the machine control strategy remains unchanged compared with the traditional one.

INDEX TERMS
Solid-rotor high-speed induction machine (IM), 2-D finite element method (FEM), asymmetric winding arrangement, current unbalance suppression, coil arrangement.

NOMENCLATURE

l_{ef}	Effective core length [mm]
$D_{s,in}$	Stator inner diameter [mm]
$D_{s,out}$	Stator outer diamerter [mm]
D_r	Solid rotor diameter [mm]
p	Number of pole pairs
Q_s	Number of stator slots
Q_r	Number of rotor slots
a	Number of parallel branches
N_s	Number of turns in series per phase
y_Q	Coil span in slot pitches
U_N	Line to line rated voltage [V]
f_s	Supply frequency [Hz]
T_N	Rated torque [Nm]
$T_{peak-peak}$	Torque ripple [Nm]
P_N	Rated power [kW]
s	Per-unit slip
$\cos\varphi$	Power factor
$I_{s,N}$	Average supply current at rated load [A]

The associate editor coordinating the review of this manuscript and approving it for publication was Xiaodong Sun.

$I_{p,N}$ Average phase current at rated load [A]
CUR Current unbalance ratio [%]
I_U Fundamental of phase U current [A]
I_V Fundamental of phase V current [A]
I_W Fundamental of phase W current [A]
CUF_- Unbalance factor of negative sequence current [%]
CUF_0 Unbalance factor of zero sequence current [%]
$\dot{I}_+$ Positive sequence current [A]
$\dot{I}_-$ Negative sequence current [A]
$\dot{I}_0$ Zero sequence current [A]
$\dot{I}_U$ Phase U current phasor [A]
$\dot{I}_V$ Phase V current phasor [A]
$\dot{I}_W$ Phase W current phasor [A]
$\dot{a}$ Phasor operator
$L_{s,U}$ Phase U stator inductance [H]
$L_{s,V}$ Phase V stator inductance [H]
$L_{s,W}$ Phase W stator inductance [H]
$L_{s\sigma,U}$ Phase U stator leakage inductance [H]
$L_{s\sigma,V}$ Phase V stator leakage inductance [H]
$L_{s\sigma,W}$ Phase W stator leakage inductance [H]

I. INTRODUCTION

High-speed solid-rotor induction machines (IMs) are capable of achieving high rotational speeds and operating in harsh environments, compared with other machines for high speed applications as permanent magnet synchronous machines (PMSMs) and switched reluctance machines (SRMs) [1]–[4]. The PMSM has a higher power density than the IM, but the cost of the machine is higher because of the expensive magnet material and the maximum speed is lower. The SRM has the advantage of the easier manufacturing, but the control becomes more difficult and the noise becomes stronger than in the IM. Therefore, high-speed IMs equipped with a solid rotor are widely used in industrial applications. The rotor of such machines is built of magnetically soft constructional steel, which offers a rugged solution compared to other rotor structures [5], [6]. Although a solid rotor is one of the most robust rotor structures, it also brings some challenges, in particular high solid-rotor losses, which make cooling of the motor challenging and expose the motor to potential machine faults [7]. Typically, there are three types of rotor losses containing the hysteresis, eddy currents, and anomalous losses, which are reported in detail in [8] and can be modeled accurately by the nonlinear lumped parameter equivalent circuit. For solid-rotor IM the majority of the rotor losses are eddy currents related losses. The main reason for the high rotor losses is the relatively low conductivity of the solid-rotor steel compared with the copper, which leads to significant slip related losses at the nominal load. In the case of a pure solid rotor with no extra windings, the high axial conductivity is needed to provide the current flow required in the rotor for torque production. The rotor material has a significant influence on solid-rotor losses, and many different types of rotor materials for high-speed applications have been investigated by researchers. Studied materials include carbon steel alloys, Fe-Si and Fe-Ni alloys, maraging steel, Fe-Co alloys and Fe-Cu alloys, as reported in [9]. Although some of the materials result in much lower rotor losses than others, in all cases the losses are still much higher than those of a machine equipped with a copper cage winding and a laminated rotor. Among the solid rotor core materials studied, Fe-Cu alloy has the lowest resistivity, which is $1.1 \times 10^{-7}\Omega$m at 20°C. This resistivity is still one order higher than the copper resistivity ($1.78 \times 10^{-8}\Omega$m).

Mitigating the solid-rotor losses by modifying the rotor itself has also been studied. For example, slitted rotors are widely used to reduce the slip related losses (caused by the fundamental of the air-gap flux density) [10]–[12]. Rotor sleeves (coatings) are highly recommended to suppress the high-frequency eddy-current losses induced by the air-gap flux density harmonics [13]–[15]. A significant share of the total solid-rotor losses are mainly caused by the air-gap flux density harmonics. Therefore, it is recommended that the stator should be designed to produce the minimal amount of the air-gap flux density harmonics. Typically, semimagnetic wedges are used in the slot openings to suppress the stator slot harmonics and double-layer short-pitch stator windings are used to mitigate the winding harmonics e.g. −5th, +7th, −11th, +13th [16], [17]. Sometimes however, the winding installation and assembly becomes very difficult when double-layer winding is used, especially in the case of prefabricated coils. In a two-pole machine, the manufacturing of a double-layer winding become very difficult as in the worst case half of the coil sides remain hanging in the stator bore leaving almost no space for the practical winding work. Therefore, using alternative techniques to the orthodox two-layer short-pitched winding becomes not just tempting but in some cases a necessity. The asymmetric winding can offer easy manufacturing, as reported in [18], [19]. But this solution comes at the cost of an asymmetric behavior of the main flux and leakage flux.

Using the asymmetric winding causes the machine to suffer some current unbalance. Such unbalance can produce harmful effects, e.g. extra losses, torque ripples, unbalanced magnetic pulls [20], [21]. Therefore, the current unbalance or impedance unbalance of the system should be mitigated as much as possible. Hu *et al.* [20], [22] utilized a compensation unit in both parallel and series to suppress the second harmonic DC-bus voltage pulsation and torque ripple caused by the asymmetric impedance in an asymmetric permanent magnet synchronous generator system. Yepes *et al.* [23] proposed an improved multiple-resonant-controller structure to compensate the current harmonics for a *n*-phase machine with an asymmetrical winding. Active power filters, as reported in [24], [25], are also very popular for compensating the current unbalance in many applications. However, all of the methods mentioned above require extra power circuit components or power electronics, which increase investment cost for the system. In addition, the control strategy also has to be modified accordingly. Furthermore, not all the proposed solutions are suitable for machines with asymmetric winding,

as some of them are designed for power systems. There is a lack of research that specially investigates current unbalance mitigation strategies for machines with inherently asymmetric windings.

The aim of this paper is to suggest methods to mitigate the current unbalance and other harmful effects (e.g. torque and speed ripples) in a high-speed solid-rotor IM, that result from the usage of an asymmetric double-layer winging arrangement. The proposed methods are based on balancing the stator inductances, as they are the main reason for the current unbalance, when the proposed winding (having much simpler manufacturing routine) is applied. The novel mitigation technique is realized by increasing the stator slot height and then optimizing the positioning of the different phase coils in different stator slots. Based on this approach, two potential methods for current unbalance mitigation are proposed and compared in this paper. The proposed methods are found to be very effective for mitigating unbalance phenomena in the machine and they are easy to implement at low cost. However, a disadvantage is that some of the machine efficiency is sacrificed because of the increment of the overall stator inductance. This efficiency can, however, be taken into account during the design phase and can be easily compensated, e.g. by slightly increasing the supply voltage.

II. HIGH-SPEED SOLIR-ROTOR IM PERFORMANCE ANALYSIS WITH ASYMMETRIC WINDING

A. ASYMMETRIC WINDING DESCRIPTION OF THE HIGH-SPEED SOLID-ROTOR IM

The machine studied is a 660 V, 2 MW, 200 Hz, 12000 r/min high-speed slitted-solid-rotor IM. Its initial design is reported in detail in [26], [27]. The more specific dimensions of the high-speed solid-rotor IM are listed in Table 1. Prefabricated coils are employed in the design, since the machine utilizes direct liquid cooling technology similar to the case reported in [28].

TABLE 1. Main dimensions of the high-speed solid-rotor IM.

Parameter	Value
Effective core length l_{ef}, mm	538
Stator inner diameter $D_{\mathrm{s,in}}$, mm	280
Stator outer diameter $D_{\mathrm{s,out}}$, mm	700
Solid rotor diameter D_{r}, mm	266
Rotor slit depth, mm	50
Number of pole pairs p	1
Number of stator slots Q_{s}	36
Number of rotor slits Q_{r}	44
Number of parallel branches a	2
Number of turns in series per phase N_{s}	6

Prefabricated coils are typically mechanically stiff and it is difficult to bend them further when inserting the coils in the slots. To guarantee the machine performance and solve the manufacturing problem at the same time, a novel asymmetric winding is proposed in this paper. The machine is a low-voltage high-power high-speed machine. Consequently, there are very limited alternatives to realize the motor winding taking the boundaries set by Faraday's law into account. With a traditional two-layer short-pitched winding, it is possible to connect the upper and lower level coil groups in parallel. In a primary asymmetric two-layer winding the parallel paths of the windings become different and, it is therefore impossible to use parallel paths similarly to the orthodox two-layer winding. In this paper, an asymmetric three-phase winding type is introduced in which all individual phase windings have identical parallel paths, enabling manufacturing of a low-voltage machine of this power and speed.

In addition, the winding must still be connected in delta, which is not favorable in the case of an asymmetric winding because it may cause some circulating currents. However, to guarantee the same amount of flux linkage as the winding in delta connection, using star connection should result in about 1200 V (660 V $\times \sqrt{3} = 1143$ V) line-to-line voltage, which makes commercial converters unavailable. Therefore, several compromises have been made to make it possible to realize a high-power high-speed low-voltage machine.

Fig. 1(a) and (b) show a comparison of the traditional and proposed double-layer winding arrangements for the high-speed solid-rotor IM. It can be seen that the asymmetric winding has different arrangements in 24 half-slots with a short pitch $y_{\mathrm{Q}} = 15/18$. The resultant current linkage per

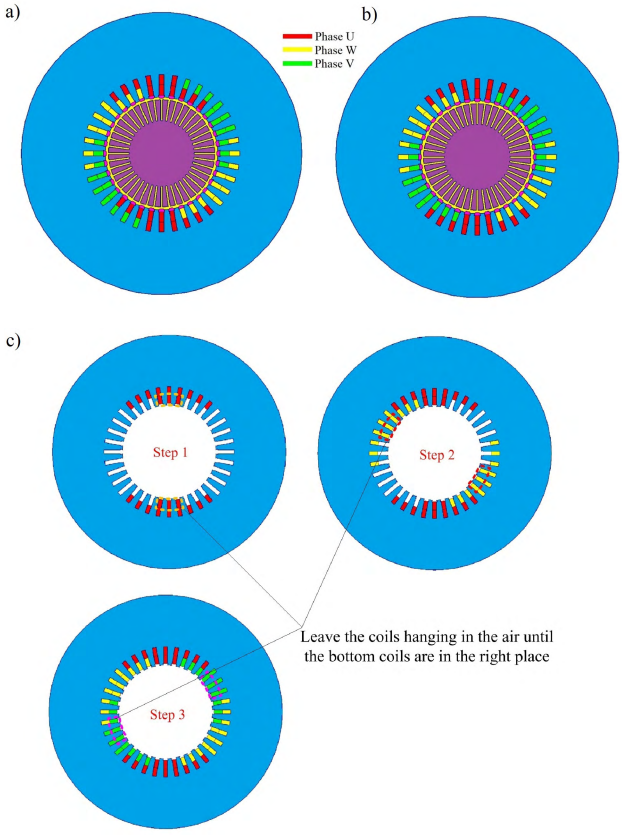

FIGURE 1. (a) The traditional double-layer stator winding arrangement. (b) The proposed asymmetric double-layer stator winding arrangement. (c) Assembly sequence of the proposed asymmetric winding.

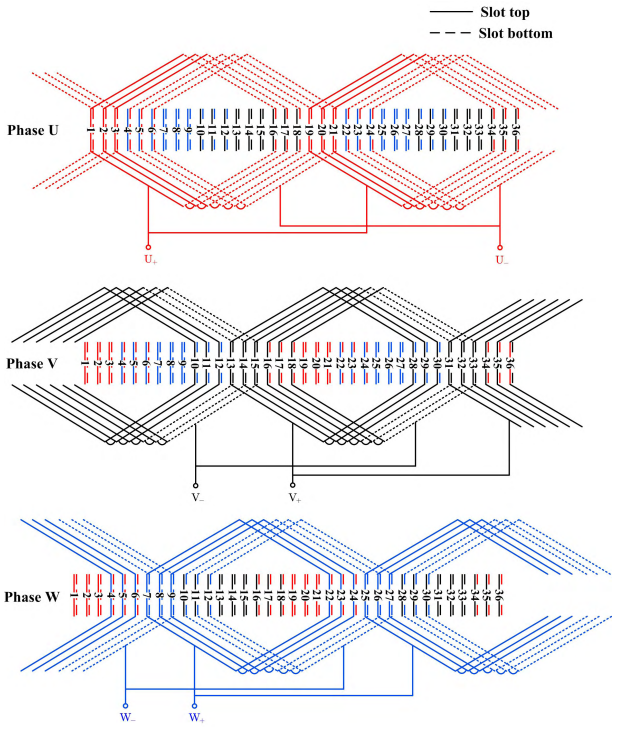

FIGURE 2. The coil arrangements for the proposed asymmetric winding.

phase is exactly the same as in a traditional winding arrangement. From the figure, it can be deduced that the three-phase stator inductances and the stator phase mutual inductances are not fully symmetric. The advantage of the proposed design is that the winding (prefabricated winding) installation becomes much easier when only a few coil sides need to be left hanging in the stator bore before the bottom coil sides are in their right places, as shown in Fig. 1(c). Detailed coil arrangements for this proposed asymmetric winding are described in Fig. 2. There are two parallel branches in the winding, and the winding is in delta connection.

Table 2 lists the main parameters and performances of the machine with the asymmetric winding at the nominal load. All the simulations in this paper are conducted by 2D FEM and the end winding effect is considered by the end winding leakage inductance (7×10^{-5} H by the analytical method) in an external circuit, which is coupled with the finite element model. Meanwhile, the ending winding resistance is added to the total winding resistance. In this table, the three-phase average phase current (phase U, V, and W currents are 1446 A, 1562 A, and 1506 A, respectively) is 1505 A, which means that the machine is suffering some asymmetry because of the proposed winding with three-phase symmetric sinusoidal voltage supply. Additionally, enhanced torque ripple can also be observed at the nominal load. The asymmetry mainly results from the asymmetric stator inductances containing the magnetizing inductance and leakage inductance, because the average position of the coils of each phase within the slot height is different. For example, the number

TABLE 2. Parameters and performances of the IM with the asymmetric winding at the nominal load.

Parameter	Value
Line to line voltage U_{N}, V	660
Connection type	Delta
Supply frequency f_{s}, Hz	200
Torque T_{N}, Nm	1600
Torque ripple $T_{\mathrm{peak-peak}}$, Nm	82
Electric power P_{N}, kW	2000
Per-unit slip s	0.00535
Power factor $\cos\varphi$	0.68
Average supply current $I_{\mathrm{s,N}}$ (RMS), A	2606
Average phase current $I_{\mathrm{p,N}}$ (RMS), A	1505
Stator copper losses, kW	5
Stator iron losses, kW	15.46
Solid rotor losses, kW	26.23
Mechanical losses, kW	10
Extra losses, kW	10
Total losses, kW	53.580
Efficiency, %	97.321

of windings positioned at the bottom of the slot for phase U is 18 and at the top of the slot is 6. Whereas, for phase V the number of windings positioned at the bottom is 6 and at the top of the slot is 18. Typically, the coil sides placed at the slot bottom generate a higher slot leakage flux and therefore higher leakage inductances compared with those located at the slot top [29]. The leakage flux path for the bottommost coils offers lower reluctance for the leakage magnetic flux than that of the topmost coils. This phenomenon is further explained in more detail in [30].

B. DEFINITIONS OF THE CURRENT UNBALANCE RATIO AND CURRENT UNBALANCE FACTOR

As there are no standardized indices to assess the current unbalance, two measures that include current unbalance ratio (CUR) and current unbalance factor (CUF) are proposed. The factors have similar definitions as the voltage unbalance described in [31], [32]. The CUR is defined as follows

$$CUR = \frac{\max\left(I_{\mathrm{U}}, I_{\mathrm{V}}, I_{\mathrm{W}}\right) - \min\left(I_{\mathrm{U}}, I_{\mathrm{V}}, I_{\mathrm{W}}\right)}{\mathrm{avg}\left(I_{\mathrm{U}}, I_{\mathrm{V}}, I_{\mathrm{W}}\right)} \times 100\% \quad (1)$$

where I_{U}, I_{V}, and I_{W} are the fundamental RMS values of phase or line currents. It can be concluded from (1) that the CUR mainly reflects the maximum current deviation with respect to the average current. Because the machine is in delta connection, the machine has positive, negative and zero sequence phase currents but only positive and negative line currents. The zero sequence phase current only travels inside the delta connection, which is regarded as the circulating current. The CUFs for negative and zero sequence currents can be expressed as

$$CUF_{-} = \frac{\dot{I}_{-}}{\dot{I}_{+}} \times 100\% \quad (2)$$

$$CUF_{0} = \frac{\dot{I}_{0}}{\dot{I}_{+}} \times 100\% \quad (3)$$

where $\dot{I}_+$, $\dot{I}_-$, and $\dot{I}_0$ are the positive, negative and zero sequence components of the phase or line currents (fundamental or harmonic currents). (2) and (3) mainly reveal the corresponding ratios with respect to the positive sequence currents. The positive, negative and zero sequence currents can be calculated as

$$\dot{I}_0 = \frac{\dot{I}_\mathrm{U} + \dot{I}_\mathrm{V} + \dot{I}_\mathrm{W}}{3} \tag{4}$$

$$\dot{I}_+ = \frac{\dot{I}_\mathrm{U} + \dot{a} \cdot \dot{I}_\mathrm{V} + \dot{a}^2 \cdot \dot{I}_\mathrm{W}}{3} \tag{5}$$

$$\dot{I}_- = \frac{\dot{I}_\mathrm{U} + \dot{a}^2 \cdot \dot{I}_\mathrm{V} + \dot{a} \cdot \dot{I}_\mathrm{W}}{3} \tag{6}$$

where $\dot{a} = 1\angle 120°$. $\dot{I}_\mathrm{U}$, $\dot{I}_\mathrm{V}$, and $\dot{I}_\mathrm{W}$ are the phase or line current phasors.

TABLE 3. Asymmetric characteristics of the machine with the asymmetric winding.

Parameter	Value
No-load phase CUR, %	6.409
No-load line CUR, %	2.613
No-load phase CUF_-, %	1.536
No-load phase CUF_0, %	2.191
No-load phase 3rd order circulating current, A	45.337
No-load line CUF_-, %	1.535
Rated-load phase CUR, %	7.683
Rated-load line CUR, %	3.377
Rated-load phase CUF_-, %	1.966
Rated-load phase CUF_0, %	2.489
Rated-load phase 3rd order circulating current, A	35.331
Rated-load line CUF_-, %	1.965
Rated-load torque ripple $T_{\mathrm{peak-peak}}$ (400 Hz), Nm	82.111

Table 3 lists asymmetric characteristics of machine with the proposed winding, without tuning machine properties. Both the phase and line current unbalance indices are shown, because the phase current unbalance is directly related to the machine performance and line current unbalance is important from the supply point of view. In Table 3, only the fundamental and the 3rd order currents are analyzed because they have higher amplitudes than other harmonics. The 3rd order related indices are marked with "3rd order". The rest of the indices without a mark are describing the fundamental currents. The 3rd order components only appear in the phase currents and the three-phase 3rd order currents have the exact same phase, which means that they are the circulating currents and they can only travel inside the delta connection. They are not capable of generating any rotating magnetic flux either, instead they create leakage flux.

There is no CUF_0 for the line current in Table 3, because the zero sequence line current is negligibly small. The machine has no neutral line (star-delta connection), which means the zero sequence impedance is infinite. It can be seen that the phase current has a higher CUR than the line current at both no load and the rated load. Since the line current has a bigger denominator when CUR is calculated by (1). Similarly, the phase current always has a higher CUF_- and CUF_0. Additionally, it can be seen from the table that the zero sequence phase current is higher than the negative sequence phase current. The zero sequence phase current can only create a pulsating magnetic flux, which will cause some extra losses. However, the negative sequence phase current is capable of generating a rotating magnetic flux that travels in the opposite direction with respect to the fundamental magnetic flux. The electromagnetic torque mainly results from the interaction of different magnetic flux harmonics. Therefore, a double supply frequency (400 Hz) torque ripple (82.111 Nm) is shown in the table because of the interaction of the fundamental and the negative sequence magnetic fluxes [20] . The torque ripple can make the control of the machine become more difficult and also increases the noise and vibration level of the machine.

III. SUPPRESSION OF THE CURRENT UNBALANCE AND PERFORMANCE ANALYSIS

The three-phase phase current (fundamental, RMS values) at the nominal load for phases U, V, and W are 1446 A, 1562 A, and 1506 A, respectively, which means that the three-phase stator inductance should be $L_{\mathrm{s,U}} > L_{\mathrm{s,W}} > L_{\mathrm{s,V}}$. The three-phase circuit has exactly the same voltage supply level and winding resistance. Therefore, the current unbalance is caused by the different stator inductances containing the magnetizing inductances and leakage inductances. In Fig. 1(b), there are 18, 6, and 12 conductors located at the slot bottom for phase U, V and W, respectively. As a result, the three-phase stator slot leakage inductance should be $L_{s\sigma,\mathrm{U}} > L_{s\sigma,\mathrm{W}} > L_{s\sigma,\mathrm{V}}$. Because the overall flux linkage (the same voltage supply) for each phase is the same, the different stator leakage inductances further indicate that the three-phase magnetizing inductances are asymmetric, which is directly related to the difference between the overall flux linkage and the flux leakage. Consequently, adjusting the slot leakage inductance for different phases separately may be a potential method to balance the three-phase current.

The method proposed in this paper to mitigate the current unbalance is arranged as follows. The main idea is to balance the three-phase inductance by reducing $L_{\mathrm{s,U}}$, and concurrently increasing $L_{\mathrm{s,V}}$ and $L_{\mathrm{s,W}}$. To be more specific, the phase U stator inductance is reduced by increasing the total magnetic circuit reluctance. For phases V and W, the stator inductances are increased by increasing the stator leakage inductances. The specific implementation is illustrated in Fig. 3. It is shown in Fig. 3(a) that the stator slot height is increased slightly giving an extra area in the slot (marked in blue). The phase U winding is placed at the slot top and phases V and W are placed at the slot bottom. Therefore, the extra slot area is located at the slot bottom for phase U and slot top for phases V and W. The extra slot area can be filled with the non-conducting nonmagnetic material, e.g. a glass-fiber stick. For the phase U, the extra slot area at the slot bottom can reduce the stator inductance because it reduces the stator yoke height which makes the overall magnetizing reluctance of the yoke higher. Phases V and W have extra slot area at the top of the slot and this slot area proposes extra paths for the leakage

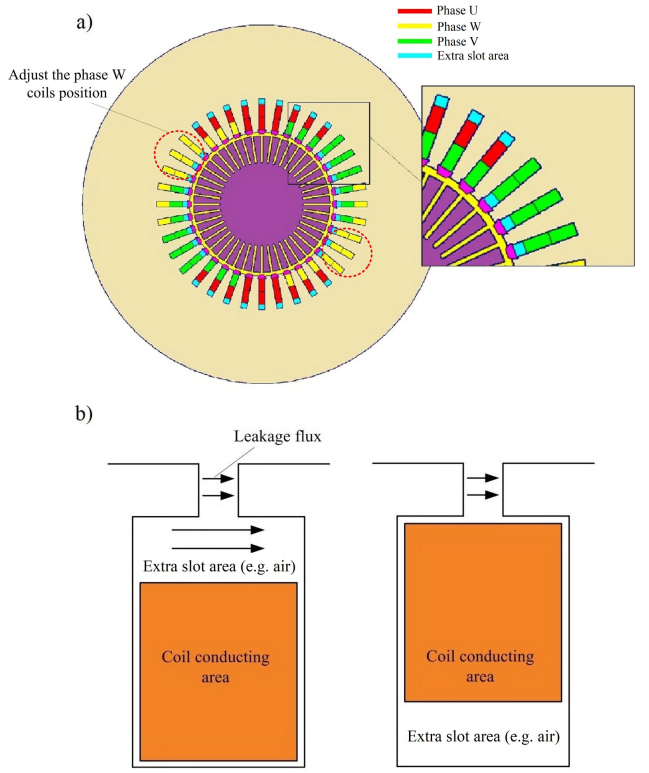

FIGURE 3. (a) Suppression of the current unbalance by modifying the coil arrangement with extra slot height. (b) Main stator slot leakage paths with different coil arrangements.

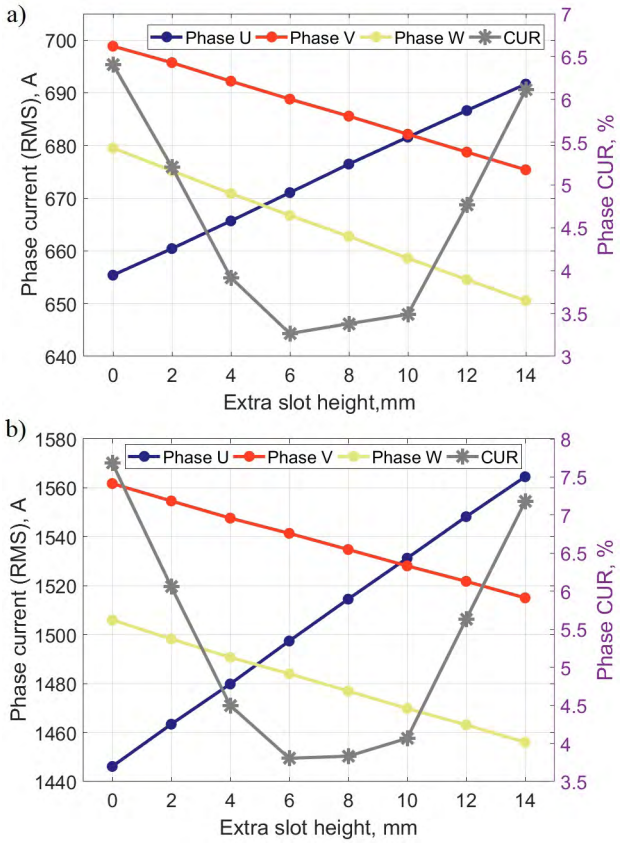

FIGURE 4. (a) No-load phase currents and CURs as a function of the extra slot height (2D FEM). (b) Rated-load phase currents and CURs as a function of the extra slot height (2D FEM).

flux to travel through, as shown in Fig. 3(b). Consequently, the corresponding stator leakage inductances will increase. Although the increased slot height for phases V and W can also reduce the magnetizing inductances (the same situation of phase U), the phases V and W total stator inductances still increase because the leakage inductance increases more. This phenomenon will be further discussed in Section III-A. It should be noted that in the design all the stator slot heights are increased by the same dimension. The stator lamination itself has an isotropic geometry in the cross-section plane, and this isotropic geometry does not complicate the stator lamination during the manufacturing process. The only difference is the winding arrangement in which the specific coils are placed at different positions in different stator slots.

Because all the three-phase stator inductances are different, it is very difficult to fully balance the three-phase stator current with three variables by a single procedure. Therefore, two possible means are studied and compared in the following sections. One possible way of balancing the currents is by placing the phase U winding at the slot top and phases V and W at the slot bottom with the extra slot areas in all the slots. Adjusting the extra slot height makes it possible to acquire the optimized dimension, when all the three-phase currents are close to each other. The other method is that based on the extra slot height adjustment results that are shown in Section III-A, and further balancing the phase W current by adjusting the coil side position in the slots, as shown in Fig. 3(a).

A. CURRENT UNBALANCE MITIGATION BY THE EXTRA STATOR SLOT HEIGHT ADJUSTMENT

To mitigate the current unbalance efficiently, the extra stator slot height can be further optimized. In this study, the extra slot height varies from 0 mm to 14 mm for the optimization. Fig. 4 shows the changes in the phase currents and phase CURs during the optimization of the extra slot height at both no load and the rated load. The figure indicates that the proposed method is very effective, because the phase U current increases with the increment of the slot height, while phase V and W currents decrease. The lowest CURs can be obtained when the extra slot height ranges from 6 mm to 10 mm. The minimum CURs are 3.266% and 3.806%, respectively, at both no load and the rated load, when the extra slot height reaches 6 mm. The situation is similar for the line current unbalance, as shown in Fig. 5. However, the best extra slot height range for smaller CURs is from 4 mm to 8 mm and the minimum CURs are 1.334% and 1.647% at 4 mm, respectively, at no load and the rated load. It can be deduced from Fig. 4 and Fig. 5 that the best range is from 6 mm to 8 mm, which makes both the phase and line CURs small.

Fig. 6 shows the details of the phase currents and CUFs at both no load and the rated load. In Fig. 6(a), the no-load positive sequence current decreases with the increment of the

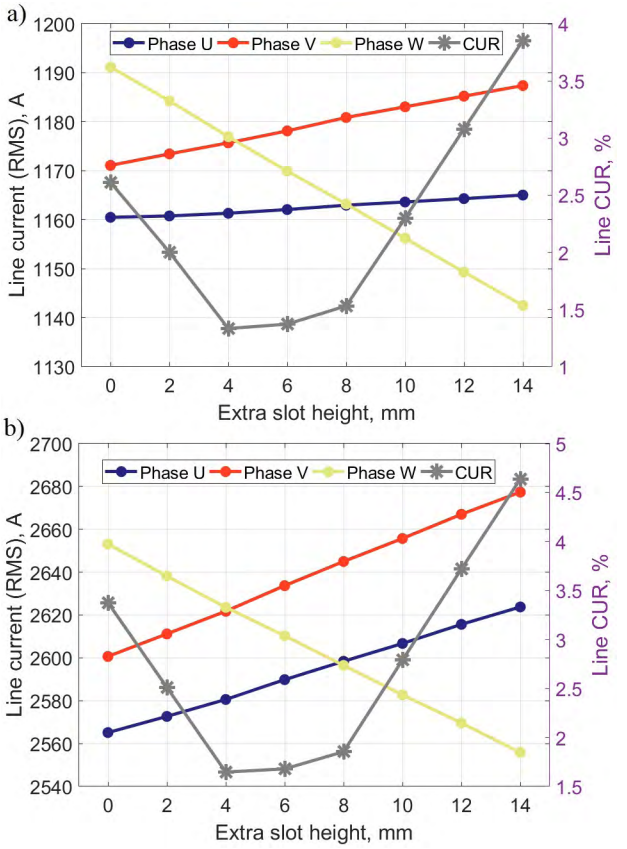

FIGURE 5. (a) No-load line currents and CURs as a function of the extra slot height (2D FEM). (b) Rated-load line currents and CURs as a function of the extra slot height (2D FEM).

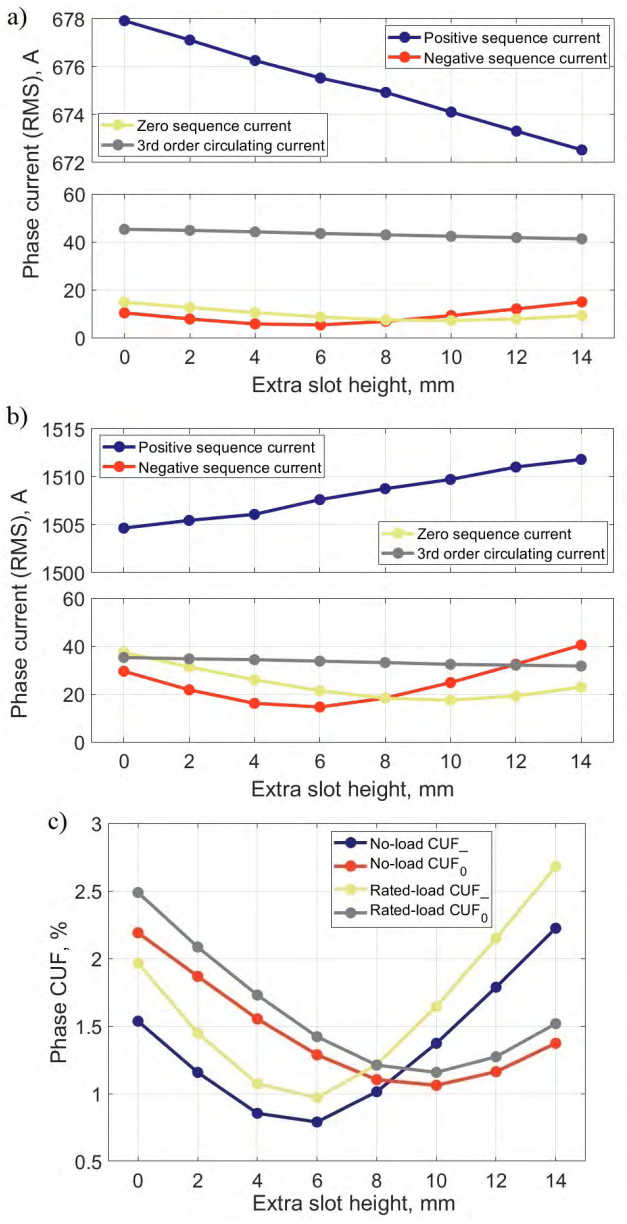

FIGURE 6. (a) No-load phase currents as a function of the extra slot height (2D FEM). (b) Rated-load phase currents as a function of the extra slot height (2D FEM). (c) CUFs as a function of the extra slot height at both no load and the rated load (2D FEM).

extra slot height, because the stator overall leakage inductance increases with larger extra slot height. Concurrently, as shown in Fig. 6(b) the positive sequence phase current increases at the rated load. The larger stator leakage inductance results in a lower air-gap magnetic flux and as a result, the motor slip will increase and a larger stator current will be seen in the stator winding. This outcome further indicates that the proposed method to mitigate the current unbalance is realized by sacrificing some of the machine performance. The proposed technique increases the stator leakage and corresponding reactive voltage drop. The extra leakage (the stator leakage inductance), however, also acts as a current filter smoothening air-gap current linkage time harmonics. The negative and zero sequence currents in both cases decrease at the beginning and increase after reaching the minima. However, the 3rd order circulating currents always decrease with the increment of the extra slot height. In addition, it can be seen in the figure that the negative and zero sequence currents at the rated load are always higher than at no load. This is because the negative and zero sequence currents belong to the fundamental current component. The heavier rated condition can always enhance the fundamental current because of the higher slip. That is to say, the asymmetry is worse under load. However the situation is inverted for the 3rd order circulating current. The 3rd order circulating current is always higher at no load, as shown in Fig. 6.

Fig. 6(c) shows the corresponding CUFs. It can be seen in the figure that the negative sequence current unbalance factor CUF_{-} reaches the minima (0.791% and 0.970%) when the extra slot height is 6 mm and the zero sequence current unbalance factor CUF_0 reaches the minima (1.287% and 1.421%) when the extra slot height is 10 mm. In addition, it also shows that when the extra slot height is small (from 0 mm to 8 mm) the CUF_0 is higher than the CUF_{-}. When the height becomes larger (from 8 mm to 14 mm), the figure shows the opposite result.

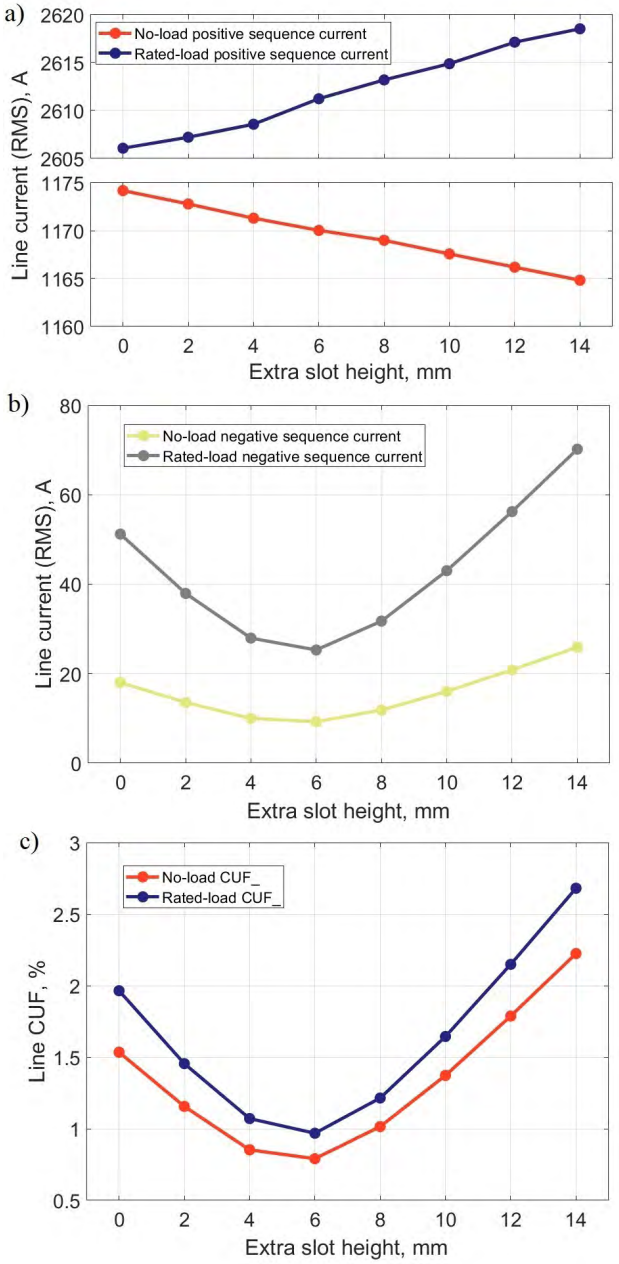

FIGURE 7. (a) Positive sequence line currents as a function of the extra slot height (2D FEM). (b) Negative sequence line currents as a function of the extra slot height (2D FEM). (c) CUFs as a function of the extra slot height at both no load and the rated load (2D FEM).

Fig. 7 shows the line current unbalance at both no load and the rated load. The positive sequence line current has the same tendency as the phase current, when the extra slot height is increased. The negative sequence line current unbalance factor CUF_ curves also show similar patterns as are seen in Fig. 6(c). The minima of the CUF_ are 0.791% and 0.969%, when the extra slot height is 6 mm.

The analysis above shows that the proposed method for mitigating the current unbalance by optimization of the extra slot height is very effective as most of the current unbalance

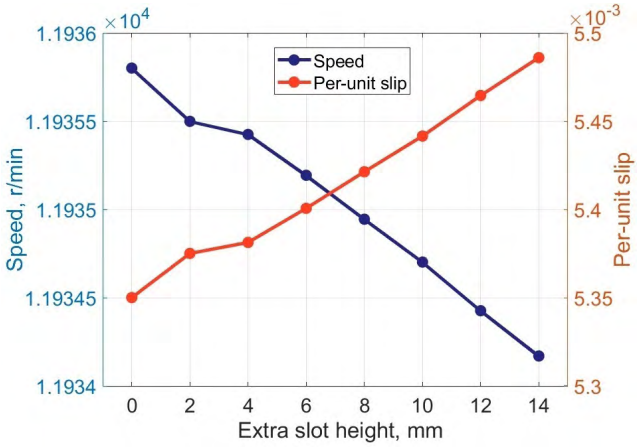

FIGURE 8. Rotating speed and per-unit slip as a function of the extra slot height with the rated torque $T_N = 1600$ Nm (2D FEM).

indices can be reduced to almost half of the initial values. The best extra slot height for the different minimum indices varies from 4 mm to 10 mm. The extra dimension can be further determined by the machine performance analysis, which is shown in the next several paragraphs.

Fig. 8 shows the rotating speed and per-unit slip varying as a function of extra slot height. The speed becomes slightly lower and the per-unit slip becomes slightly higher when the slot height is increased. This result indicates that the positive magnetizing flux is smaller with a bigger slot height, since with a smaller magnetizing flux, the machine runs at a lower speed to create the rotor current needed for the same torque. Based on the fundamental behavior of the machine, it can consequently be deduced that the rotor losses may be increased slightly. This feature can however be taken into account and compensated in the machine dimensioning.

The corresponding machine losses as a function of the extra slot height are illustrated in Fig. 9. The solid-rotor losses, stator core losses and copper losses are all estimated by the 2-D FEM. The mechanical losses and extra losses in Table 2 are considered as constants at the rated load and they have been taken into account in the efficiency calculation. In Fig. 9(a), the solid-rotor losses increase because of the higher per-unit slip. The stator core losses and copper losses also increase because more stator leakage is generated in the stator core and a higher slip brings higher copper losses. As a result, the efficiency decreases with the increment of the slot height. This phenomenon exactly shows that the proposed method sacrifices the efficiency to mitigate the current unbalance. This is an interesting result as the original hypothesis was that the negative sequence currents should cause more losses in the machine.

Fig. 10 describes the torque ripple (400 Hz) as a function of the extra slot height at the rated load. It can be seen that it drops at the beginning and reaches a minimum of 41.242 Nm at 6 mm. After that it increases with the increment of the slot height. The double supply frequency torque ripple mostly

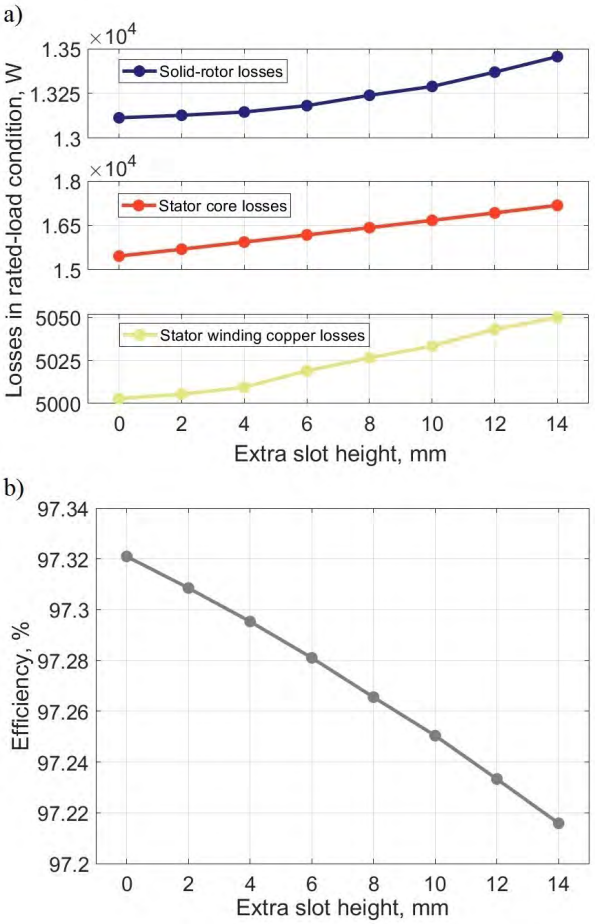

FIGURE 9. (a) Machine main losses as a function of extra slot height with the rated torque $T_N = 1600$ Nm (2D FEM). (b) Machine efficiency as a function of the extra slot height with the rated torque $T_N = 1600$ Nm (2D FEM).

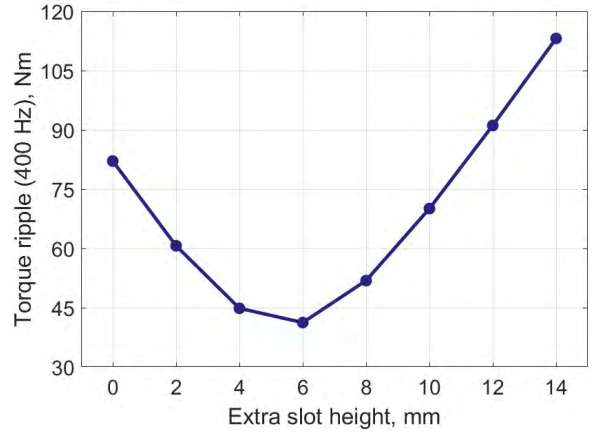

FIGURE 10. Torque ripple as a function of the extra slot height with the rated torque $T_N = 1600$ Nm (2D FEM).

depends on the negative sequence rotating magnetic flux, which is directly related to the negative sequence current as illustrated in Fig. 6. Therefore, it can be seen that the negative sequence current and the torque ripple have the similar curves

TABLE 4. Asymmetric characteristics with the optimized extra slot height.

Parameter	Value	Red. rate
Extra slot height, mm	6	–
No-load phase CUR, %	3.266	0.490
No-load line CUR, %	1.372	0.475
No-load phase CUF_{-}, %	0.791	0.485
No-load phase CUF_0, %	1.287	0.413
No-load phase 3rd order circulating current, A	43.566	0.039
No-load line CUF_{-}, %	0.791	0.485
Rated-load phase CUR, %	3.806	0.505
Rated-load line CUR, %	1.679	0.503
Rated-load phase CUF_{-}, %	0.970	0.507
Rated-load phase CUF_0, %	1.421	0.429
Rated-load phase 3rd order circulating current, A	33.803	0.043
Rated-load line CUF_{-}, %	0.969	0.507
Rated-load torque ripple $T_{peak-peak}$, Nm	42.242	0.486
Efficiency, %	97.250	–

(the same tendency with the increment of the slot height).

Based on the data evaluating the current unbalance and machine performances the shown in the figures a 6 mm extra slot height was selected as the best solution. This value brings very small current unbalance indices (some of them are the minimum) and the minimum torque ripple. The corresponding data are listed in Table 4. The "Red. rate" in this table denotes the reduction rate with respect to the initial case without any extra slot height modification. The values in the table show that the proposed method is effective and most of the current unbalance indices and torque ripple are reduced by about a half. The effect is quite limited for mitigating the phase 3rd order circulating currents at both no load and the rated load, because they are only reduced by around 4%. However the 3rd order circulating currents always exist when a delta connection is used, even in the machine with a fully symmetric winding. All these benefits of smaller the current unbalance and torque ripples are gained by sacrificing the machine efficiency. The machine suffers extra losses of 1.4 kW in total, which reduces the efficiency from 97.321% to 97.250%. This efficiency drop is acceptable because it makes the machine control easier due to the steadier out-put torque and more even converter out-put currents. Additionally, the noise and vibration of the machine is also further suppressed.

B. CURRENT UNBALANCE MITIGATION BY THE COIL SIDE POSITION ADJUSTMENT IN THE STATOR SLOT FOR PHASE W

Based on the phase current curves in Fig. 4, the current unbalance can be further mitigated by adjusting the phase W coil side position. In Fig. 4, there are intersections of the phase currents at both no load and the rated load, when extra slot height is 10 mm. It is possible to get a fully balanced phase current by adjusting the coil side position of phase W, as shown in Fig. 3(a). In the figure the positions of only some coils are recommended to be adjusted, because the coils in other stator slots do not belong to a single phase W. The analysis in Section III-A indicates that most of the indices

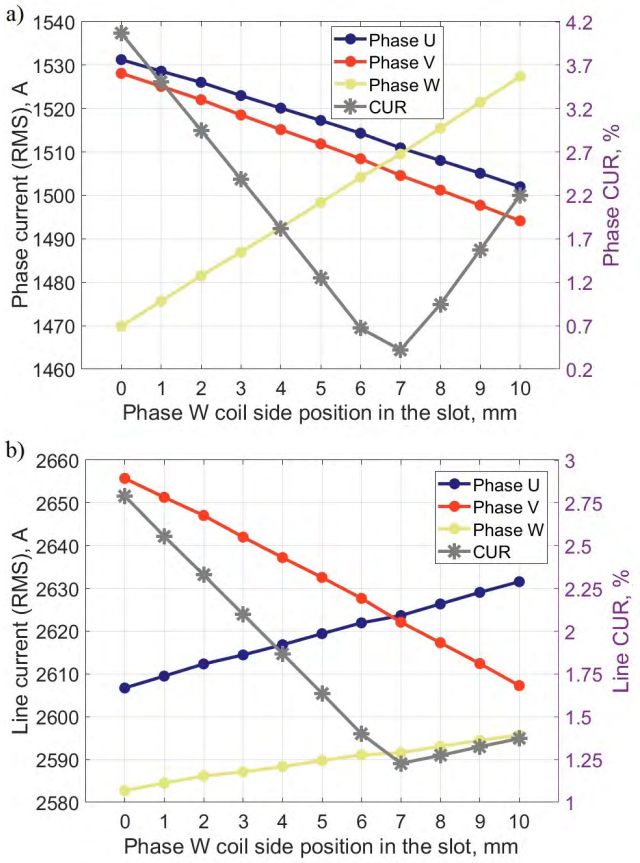

FIGURE 11. (a) Phase currents and CURs as a function of the coil side position of phase W in the stator slot at the rated load with 10 mm extra slot height (2D FEM). (b) Line currents and CURs as a function of the coil side position of phase W in the stator slot at the rated load with 10 mm extra slot height (2D FEM).

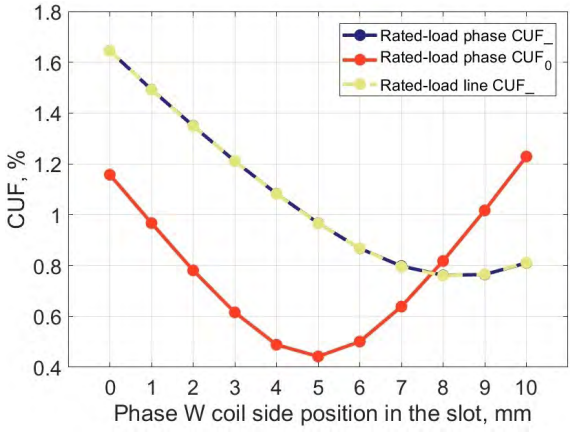

FIGURE 12. Phase and line CUFs as a function of the coil side position of phase W in the stator slot at the rated load with 10 mm extra slot height (2D FEM).

TABLE 5. Asymmetry winding coil side position in the stator slot.

Slot number	34-6	7-9	10-15	16-24	25-27	28-33
Phase	U,V,W	W	V,W	U,V,W	W	V,W
Position, mm	10	7	0	10	7	0

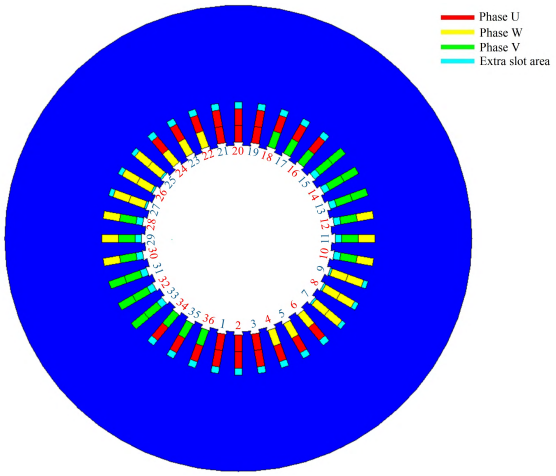

FIGURE 13. Coil arrangements for the three-phase asymmetric winding in different stator slots.

at the rated load have a good agreement with those at no load. Therefore, only the rated current unbalance indices are considered during the optimization of the phase W coil side position.

The adjustment of the coil side position is carried out after choosing a extra slot height of 10 mm, because the three-phase current intersections only show in that situation. Fig. 11 illustrates the three-phase current and CURs as a function of the coil side position of phase W in the stator slot at the rated load. It is assumed that the coil side position is 0 mm when the coil side is placed in the slot bottom, as shown in Fig. 3(a). It can be seen in Fig. 11(a) that the three-phase phase current (fundamental, RMS value, 1511 A, 1505 A, and 1510 A) gets very close to each other when the coil side position is 7 mm and the CUR reaches the minimum of 0.422% at the same time. The same conclusion can be drawn for the three-phase line current and CUR. The currents are 2624 A, 2622 A, and 2592 A, respectively, and the CUR is 1.227% when the coil side position in the stator slot is 7 mm.

Fig. 12 shows phase and line CUFs as a function of the coil side position of phase W in the stator slot at the rated load with 10 mm extra slot height. It can be seen in this figure that the phase and line CUF$_-$ curves coincide with each other. A very small CUF$_-$ can be achieved when coil side position varies from 7 mm to 10 mm. However, the phase CUF$_0$ reaches the minimum when the coil side position is 5 mm. Based on the analysis in Section III-A, it can be concluded that the CUF$_-$ is related to the torque ripple and CUF$_0$ is more related to the losses. The machine is very sensitive to CUF$_-$, which is shown in Fig. 7 and Fig. 10. It was decided to select the 7 mm coil side position as the best solution taking the results in Fig. 11 and Fig. 12 into consideration.

Table 5 lists the specific coil arrangements for the proposed asymmetric winding with 10 mm extra slot height. The slot number is defined in Fig. 2. The more specific

TABLE 6. Asymmetric characteristics with the optimized coil side position.

Parameter	Value	Red. rate
Extra slot height, mm	10	–
Coil side position, mm	7	–
No-load phase CUR, %	0.203	0.968
No-load line CUR, %	1.012	0.613
No-load phase CUF_{-}, %	0.572	0.628
No-load phase CUF_0, %	0.670	0.694
No-load phase 3rd order circulating current, A	43.210	0.047
No-load line CUF_{-}, %	0.659	0.571
Rated-load phase CUR, %	0.422	0.945
Rated-load line CUR, %	1.227	0.637
Rated-load phase CUF_{-}, %	0.798	0.594
Rated-load phase CUF_0, %	0.639	0.743
Rated-load phase 3rd order circulating current, A	33.397	0.055
Rated-load line CUF_{-}, %	0.796	0.595
Rated-load torque ripple $T_{\mathrm{peak-peak}}$, Nm	34.604	0.579
Efficiency, %	97.255	–

coil arrangements for the three-phase asymmetric winding in different stator slots are illustrated in Fig. 13. Table 6 lists the main current unbalance indices and machine performances with the coil side position of 7 mm for phase W when the extra slot height is 10 mm. In this table, all the current unbalance indices are smaller than those in Table 4, which means that this method gives better results than only adjusting the extra slot height. From the machine point of view, the phase CURs are very small, which means that the phase currents are almost balanced. In addition, the torque ripple is further suppressed and the efficiency (97.255%) is slightly higher than in the previous method (97.250%).

IV. CONCLUSION

An asymmetric double-layer short-pitch winding with prefabricated coils was proposed for a 660 V, 2 MW, 12000 r/min high-speed solid-rotor IM. The purpose of using this winding arrangement was to make the winding manufacture and assembly easier. The proposed asymmetric winding had the disadvantage of generating asymmetric three-phase stator inductances containing magnetizing and leakage inductances, which caused some three-phase current unbalance. The current unbalance brought side effects for the machine and the converter, e.g. control difficulty, torque ripple, and noise and vibration, which should be mitigated as much as possible.

Indices including CUR and CUF were proposed in this paper to evaluate the current unbalance. Two methods were then proposed to mitigate the current unbalance. One was realized by modifying the stator slot height and placing the coils at the slot top or bottom for different phases. The other one was to further adjust the coil side position for phase W, after the slot height was optimized. Consequently, the stator inductances were adjusted successfully as requested by these two methods. As a result, all the corresponding current indices and torque ripple were reduced dramatically. These benefits were realized by at a cost of some extra losses and the machine efficiency dropped from 97.321% to 97.250% and 97.255%, respectively, for these two methods. The second method was capable of acquiring more balanced currents, a smoother torque and a higher efficiency than the first method. The proposed method has the potential to be further utilized for other types of asymmetric windings and machines to guarantee the smaller current unbalance.

ACKNOWLEDGMENT

The authors would like to thank Peter Jones, Lappeenranta University of Technology, for his help with English language of the manuscript.

REFERENCES

[1] D. Gerada, A. Mebarki, N. L. Brown, C. Gerada, A. Cavagnino, and A. Boglietti, "High-speed electrical machines: Technologies, trends, and developments," *IEEE Trans. Ind. Electron.*, vol. 61, no. 6, pp. 2946–2959, Jun. 2014.

[2] Z. Shi, X. Sun, Y. Cai, Z. Yang, G. Lei, Y. Guo, and J. Zhu, "Torque analysis and dynamic performance improvement of a PMSM for EVs by skew angle optimization," *IEEE Trans. Appl. Supercond.*, vol. 29, no. 2, pp. 1–5, Mar. 2019.

[3] X. Sun, K. Diao, G. Lei, Y. Guo, and J. Zhu, "Study on segmented-rotor switched reluctance motors with different rotor pole numbers for BSG system of hybrid electric vehicles," *IEEE Trans. Veh. Technol.*, vol. 68, no. 6, pp. 5537–5547, Jun. 2019.

[4] X. Sun, B. Su, S. Wang, Z. Yang, G. Lei, J. Zhu, and Y. Guo, "Performance analysis of suspension force and torque in an IBPMSM with V-shaped PMs for flywheel batteries," *IEEE Trans. Magn.*, vol. 54, no. 11, Nov. 2018, Art. no. 8105504.

[5] J. F. Gieras and J. Saari, "Performance calculation for a high-speed solid-rotor induction motor," *IEEE Trans. Ind. Electron.*, vol. 59, no. 6, pp. 2689–2700, Jun. 2012.

[6] J. Pyrhonen, J. Nerg, P. Kurronen, and U. Lauber, "High-speed high-output solid-rotor induction-motor technology for gas compression," *IEEE Trans. Ind. Electron.*, vol. 57, no. 1, pp. 272–280, Jan. 2010.

[7] M. Fratila, A. Benabou, A. Tounzi, and M. Dessoude, "Calculation of iron losses in solid rotor induction machine using FEM," *IEEE Trans. Magn.*, vol. 50, no. 2, pp. 825–828, Feb. 2014.

[8] X. Sun, Y. Shen, S. Wang, G. Lei, Z. Yang, and S. Han, "Core losses analysis of a novel 16/10 segmented rotor switched reluctance BSG motor for HEVs using nonlinear lumped parameter equivalent circuit model," *IEEE/ASME Trans. Mechatronics*, vol. 23, no. 2, pp. 747–757, Apr. 2018.

[9] T. Aho, V. Sihvo, J. Nerg, and J. Pyrhonen, "Rotor materials for medium-speed solid-rotor induction motors," in *Proc. IEEE Int. Electr. Mach. Drives Conf.*, vol. 1, May 2007, pp. 525–530.

[10] M. Jagiela and T. Garbiec, "Evaluation of rotor-end factors in solid-rotor induction motors," *IEEE Trans. Magn.*, vol. 48, no. 1, pp. 137–142, Jan. 2012.

[11] S. L. Ho, S. Niu, and W. N. Fu, "A novel solid-rotor induction motor with skewed slits in radial and axial directions and its performance analysis using finite element method," *IEEE Trans. Appl. Supercond.*, vol. 20, no. 3, pp. 1089–1092, Jun. 2010.

[12] M. O. Gulbahce, D. T. Mcguiness, and D. A. Kocabas, "Shielded axially slitted solid rotor design for high-speed solid rotor induction motors," *IET Electr. Power Appl.*, vol. 12, no. 9, pp. 1371–1377, Nov. 2018.

[13] J.-X. Shen, H. Hao, M.-J. Jin, and C. Yuan, "Reduction of rotor eddy current loss in high speed PM brushless machines by grooving retaining sleeve," *IEEE Trans. Magn.*, vol. 49, no. 7, pp. 3973–3976, Jul. 2013.

[14] H.-W. Jun, J. Lee, H.-W. Lee, and W.-H. Kim, "Study on the optimal rotor retaining sleeve structure for the reduction of eddy-current loss in high-speed SPMSM," *IEEE Trans. Magn.*, vol. 51, no. 3, Mar. 2015, Art. no. 8103004.

[15] J.-H. Ahn, C. Han, C.-W. Kim, and J.-Y. Choi, "Rotor design of high-speed permanent magnet synchronous motors considering rotor magnet and sleeve materials," *IEEE Trans. Appl. Supercond.*, vol. 28, no. 3, Apr. 2018, Art. no. 5201504.

[16] M. J. Islam and R. R. Moghaddam, "Loss reduction in a salient pole synchronous machine due to magnetic slot wedge and semiclosed stator slots," in *Proc. 13th Int. Conf. Elect. Mach. (ICEM)*, Sep. 2018, pp. 1267–1272.

[17] L. Huang, Z. Q. Zhu, J. Feng, S. Guo, and J. X. Shi, "Comparative analysis of variable flux reluctance machines with double- and single-layer concentrated armature windings," *IEEE Trans. Ind. Appl.*, vol. 55, no. 2, pp. 1505–1515, Mar./Apr. 2019.
[18] Y. Demir and M. Aydin, "A novel dual three-phase permanent magnet synchronous motor with asymmetric stator winding," *IEEE Trans. Magn.*, vol. 52, no. 7, Jul. 2016, Art. no. 8105005.
[19] Y. Demir and M. Aydin, "A novel asymmetric and unconventional stator winding configuration and placement for a dual three-phase surface PM motor," *IEEE Trans. Magn.*, vol. 53, no. 11, Nov. 2017, Art. no. 8111805.
[20] Y. Hu, Z. Q. Zhu, and M. Odavic, "Compensation of unbalanced impedance of asymmetric wind power PMSG compensated by external circuits in series," *CES Trans. Elect. Mach. Syst.*, vol. 1, no. 2, pp. 180–188, Jun. 2017.
[21] Z. Q. Zhu, M. L. M. Jamil, and L. J. Wu, "Influence of slot and pole number combinations on unbalanced magnetic force in PM machines with diametrically asymmetric windings," *IEEE Trans. Ind. Appl.*, vol. 49, no. 1, pp. 19–30, Jan./Feb. 2013.
[22] Y. Hu, Z. Q. Zhu, and M. Odavic, "An improved method of DC bus voltage pulsation suppression for asymmetric wind power PMSG systems with a compensation unit in parallel," *IEEE Trans. Energy Convers.*, vol. 32, no. 3, pp. 1231–1239, Sep. 2017.
[23] A. G. Yepes, J. Doval-Gandoy, F. Baneira, D. Pérez-Estévez, and O. López, "Current harmonic compensation for *n* -phase machines with asymmetrical winding arrangement and different neutral configurations," *IEEE Trans. Ind. Appl.*, vol. 53, no. 6, pp. 5426–5439, Nov./Dec. 2017.
[24] P. Verdelho and G. D. Marques, "An active power filter and unbalanced current compensator," *IEEE Trans. Ind. Electron.*, vol. 44, no. 3, pp. 321–328, Jun. 1997.
[25] G. M. Lee, D.-C. Lee, and J.-K. Seok, "Control of series active power filters compensating for source voltage unbalance and current harmonics," *IEEE Trans. Ind. Electron.*, vol. 51, no. 1, pp. 132–139, Feb. 2004.
[26] C. Di, I. Petrov, and J. J. Pyrhönen, "Modeling and mitigation of rotor eddy-current losses in high-speed solid-rotor induction machines by a virtual permanent magnet harmonic machine," *IEEE Trans. Magn.*, vol. 54, no. 12, pp. 1–12, Dec. 2018.
[27] C. Di, I. Petrov, and J. Pyrhönen, "Extraction of rotor eddy-current harmonic losses in high-speed solid-rotor induction machines by an improved virtual permanent magnet harmonic machine model," *IEEE Access*, vol. 7, pp. 27746–27755, 2019.
[28] P. Lindh, I. Petrov, A. Jaatinen-Värri, A. Grönman, M. Martinez-Iturralde, M. Satrústegui, and J. Pyrhönen, "Direct liquid cooling method verified with an axial-flux permanent-magnet traction machine prototype," *IEEE Trans. Ind. Electron.*, vol. 64, no. 8, pp. 6086–6095, Aug. 2017.
[29] M. van der Geest, H. Polinder, J. A. Ferreira, and D. Zeilstra, "Current sharing analysis of parallel strands in low-voltage high-speed machines," *IEEE Trans. Ind. Electron.*, vol. 61, no. 6, pp. 3064–3070, Jun. 2014.
[30] J. Pyrhonen, T. Jokinen, and V. Hrabovcova, *Design of Rotating Electrical Machines*. Hoboken, NJ, USA: Wiley, 2013.
[31] P. Pillay and M. Manyage, "Definitions of voltage unbalance," *IEEE Power Eng. Rev.*, vol. 21, no. 5, pp. 50–51, May 2001.
[32] *IEEE Guide for Self-Commutated Converters*, IEEE Standard 936-1987, 1987, pp. 1–42.

CHONG DI was born in Wuxi, China, in 1991. He received the B.Eng. and M.Eng. degrees in electrical engineering from the Hefei University of Technology, Hefei, China, in 2014 and 2017, respectively. He is currently pursuing the Ph.D. degree with the Department of Electrical Engineering, Lappeenranta University of Technology, Finland.

His research interest includes high-speed electrical machines.

ILYA PETROV received the D.Sc. degree from the Lappeenranta University of Technology (LUT), Finland, in 2015, where he is currently a Fellow Researcher with the Department of Electrical Engineering.

JUHA J. PYRHÖNEN (M'06–SM'17) was born in Kuusankoski, Finland, in 1957. He received the D.Sc. degree from the Lappeenranta University of Technology (LUT), Finland, in 1991.

He became a Professor of electrical machines and drives with LUT, in 1997. He is involved in the research and development of electric motors and power-electronic-controlled drives. He has wide experience in the research and development of special electric drives for distributed power production, traction, and high-speed applications. Permanent magnet materials and applying them in machines have an important role in his research. Currently, he is also studying possibilities of using carbon-based materials in electrical machines.